RESEARCH ARTICLE

Proteome analysis of porcine epidemic diarrhea virus (PEDV)-infected Vero cells

*Songlin Zeng**, *Huan Zhang**, *Zhen Ding, Rui Luo, Kang An, Lianzeng Liu, Jing Bi, Huanchun Chen, Shaobo Xiao and Liurong Fang*

State Key Laboratory of Agricultural Microbiology, College of Veterinary Medicine, Huazhong Agricultural University, Wuhan, P. R. China

Received: September 28, 2014
Revised: December 4, 2014
Accepted: January 16, 2015

Porcine epidemic diarrhea virus (PEDV) causes an acute, highly contagious, and devastating viral enteric disease with a high mortality rate in suckling pigs. A large-scale outbreak of PED occurred in China in 2010, with PEDV emerging in the United States in 2013 and spreading rapidly, posing significant economic and public health concerns. In this study, LC–MS/MS coupled to iTRAQ labeling was used to quantitatively identify differentially expressed cellular proteins in PEDV-infected Vero cells. We identified 49 differentially expressed cellular proteins, of which 8 were upregulated and 41 downregulated. These differentially expressed proteins were involved in apoptosis, signal transduction, and stress responses. Based on these differentially expressed proteins, we propose that PEDV might utilize apoptosis and extracellular signal regulated kinases pathways for maximum viral replication. Our study is the first attempt to analyze the protein profile of PEDV-infected cells by quantitative proteomics, and we believe our findings provide valuable information with respect to better understanding the host response to PEDV infection.

Keywords:
Differentially expressed proteins / iTRAQ / Microbiology / Porcine epidemic diarrhea virus (PEDV) / Quantitative proteomics

Additional supporting information may be found in the online version of this article at the publisher's web-site

1 Introduction

Porcine epidemic diarrhea (PED) is an acute and highly contagious enteric disease of pigs. Typical clinical symptoms of PED include watery diarrhea, vomiting, dehydration, and high mortality in suckling pigs [1]. This disease was first reported in feeder and fattening swine in the United Kingdom in 1971 [2], after which the causative agent PED virus (PEDV) was identified as a coronavirus [3]. Since then, outbreaks of PED have subsequently been documented in European and Asian countries, resulting in severe economic losses to the swine industry [1].

The prevalence of PED was relatively low until 2010, probably because a PED vaccine was widely used throughout China [4]. However, since December 2010, large-scale outbreaks of diarrhea with 80–100% morbidity and 50–90% mortality in suckling piglets have occurred in most Chinese provinces, affecting even vaccinated pigs [5, 6]. Investigations indicated that these large-scale outbreaks of diarrhea were caused by a variant of PEDV [7, 8]. New PEDV outbreaks have also occurred in Vietnam, Thailand, Korea, and the United States,

Correspondence: Professor Liurong Fang, Laboratory of Animal Virology, College of Veterinary Medicine, Huazhong Agricultural University, 1 Shi-zi-shan Street, Wuhan 430070, Hubei, P. R. China
E-mail: fanglr@mail.hzau.edu.cn
Fax: +86-27-8728-2608

Abbreviations: 14-3-3 gamma, tyrosine 3-monooxygenase/tryptophan 5-monooxygenase activation protein, gamma; **CPE**, cytopathic effect; **ERK**, extracellular signal regulated kinases; **HIV**, human immunodeficiency virus; **hpi**, h postinfection; **HSDL2**, hydroxysteroid dehydrogenase like 2; **IFA**, immunofluorescence assay; **IPA**, Ingenuity Pathway Analysis; **PED**, porcine epidemic diarrhea; **PEDV**, porcine epidemic diarrhea virus; **SARS-CoV**, severe acute respiratory syndrome coronavirus

*These authors contributed equally to this work.
Colour Online: See the article online to view Figs. 1 and 3 in colour.

where PEDV was considered an exotic before 2013. The PEDV variant has emerged and spread rapidly in the United States since May 2013 [9, 10]. By the end of April 2014, PEDV outbreaks had been reported in 27 states of the United States, with 2692 confirmed cases (www.aasv.org/news/story.php?id = 6989), resulting in significant economic and public health concerns.

Despite years of intensive research, the mechanisms of PEDV pathogenesis and immunomodulation remain largely unknown [11]. Emerging technologies, such as proteomic approaches, have become important tools for facilitating a comprehensive characterization of virus–host interactions involved in infection and pathogenesis [12, 13]. Several quantitative proteomics approaches have been used to provide specific insights into the gene expression profiles of coronaviruses including severe acute respiratory syndrome coronavirus (SARS-CoV) [14], infectious bronchitis coronavirus [15], and transmissible gastroenteritis coronavirus [16]. Generally, in host cells coronavirus infection gives rise to alterations in transcriptional patterns, the cell cycle, the cytoskeleton, apoptosis pathways, the immune system, stress responses, and likely also causes inflammation [17]. More data related to the host response to coronavirus infection should shed some light on potential targets for antiviral agents.

To date, proteomics has not yet been applied to analyze whole cell changes caused by PEDV infection. Since Hofmann and Wyler [18] reported for the first time that PEDV could be successfully propagated in Vero cell cultures, Vero cells have been widely used for PEDV isolation, propagation, vaccine production, and basic research. In this study, we used iTRAQ coupled with LC−MS/MS to quantitate and identify cellular proteins that were differentially expressed in Vero cells following infection with PEDV.

2 Materials and methods

2.1 Vero cell culture and PEDV preparation

African green monkey kidney (Vero) cells were purchased from the American Type Culture Collection (ATCC). Cells were cultured in DMEM (Invitrogen, Carlsbad, CA, USA) containing 10% FBS and 1% penicillin–streptomycin at 37°C/5% CO_2. The Chinese PEDV strain AJ1102 (GenBank Accession No. JX188454) used in this study was isolated in 2011 from the intestine of a suckling piglet with acute diarrhea [5]. Virus stock was harvested in Vero cells and virus titer was $10^{6.4}$ PFU/mL determined by plaque assays.

2.2 Virus inoculation

Monolayers of Vero cells were grown to 80% confluence in 10 cm^2 cell culture dishes. Culture medium was removed and monolayers gently washed with serum-free DMEM prior to inoculation. Cells incubated in serum-free DMEM containing 10 μg/mL trypsin (Promega) were inoculated with PEDV strain AJ1102 at a multiplicity of infection of 0.1. Uninfected cells served as the mock-infected group. Infected and mock groups were collected as biological replicates from three independent experiments at 24 h postinfection (hpi). Viral propagation was confirmed by the observation of cytopathic effect (CPE) and indirect immunofluorescence assay (IFA) using a monoclonal antibody against PEDV nucleocapsid (N) protein. This monoclonal antibody was produced from hybridoma cells derived from Sp2/0 myeloma cells and spleen cells of BALB/c mice immunized with recombinant N protein of PEDV strain AJ1102.

2.3 Protein extraction, digestion, and labeling with iTRAQ reagents

Cultures of PEDV-infected and control cells, including three independent biological replicates, were collected using a cell scraper, centrifuged (300 × *g*, 10 min), and washed twice with ice-cold PBS containing 1 mM pervanadate and 1 mM sodium fluoride. Cell pellets were resuspended in 500 μL of lysis buffer (7 M urea, 2 M thiourea, 4% CHAPS, 40 mM Tris-HCl, pH 8.5) containing 1 mM PMSF, 2 mM EDTA, and 10 mM DTT. Further protein solubilization was achieved by sonicating, with cellular debris removed by centrifugation (25 000 × *g*, 20 min, 4°C). The protein concentration in supernatants was quantified using the Bradford protein assay. We digested 100 μg of each sample at 37°C for 12 h with sequencing grade modified trypsin (Promega, Madison, WI, USA). Mock-infected samples were labeled with iTRAQ 113 (IT113), iTRAQ 116 (IT116), or iTRAQ 119 (IT119), and PEDV-infected samples were labeled with iTRAQ 114 (IT114), iTRAQ 118 (IT118), or iTRAQ 121 (IT121). The labeled digests were then pooled and vacuum-dried.

2.4 SCX chromatography

Peptide mixtures were loaded onto an UltremexSCX column (4.6 × 250 mm) and separated by SCX chromatography using a 20AB HPLC system (Shimadzu, Kyoto, Japan). The labeled peptides were eluted with 4 mL of buffer A (25 mM NaH_2PO_4 in 25% (ACN), pH 2.7) for 10 min, followed by a linear gradient of 5–35% and 35–80% buffer B (25 mM NaH_2PO_4, 1 M KCl in 25% ACN, pH 2.7) for 11 and 1 min at 1 mL/min, respectively. The process of elution was monitored by the absorbance at 214 nm. A total of 20 fractions that were desalted with a StrataX desalting column were collected and lyophilized in a vacuum concentrator.

2.5 MS/MS analysis

The equal amounts of digested proteins were dissolved in buffer A (2% ACN, 0.1% formic acid) at the final concentration of 0.25 μg/μL and analyzed in an LC-MS/MS system. After that, 9 μL supernatant was loaded on a Symmetry C18 trapping column (5 μm particles, 180 μm inner diameter × 20 mm; Waters) with the nanoACQUITY Sample Manager (Waters) and the peptides were eluted from the trapping column over a BEH 130 C18 column (1.7 μm particles, 100 μm inner diameter × 100 mm). The samples were loaded at 2 μL/min for 15 min, and then gradient run at 300 nL/min were from 5 to 35% buffer B (98% ACN, 0.1% formic acid) in 40 min followed by a wash for 5 min at 80% B and a 2-min equilibration step. MS/MS was performed with a Triple TOF 5600 mass spectrometer (AB Sciex, Concord, ON). The ion source was a NanoSpray III source (AB Sciex), and the radiator was a needle made of quartz (New Objectives, Woburn, MA, USA). During data acquisition, the spray voltage was set to 2.5 kV, the temperature of the interface heater was 150°C, with the curtain gas 30 pounds per square inch. Survey scans were acquired in 250 ms and 30 product ion scans were collected under the condition of exceeding the threshold of 120 counts per second (counts/s). Total cycle time was fixed to 3.3 s. Dynamic exclusion was set for half of peak width (18 s), and the fragmentation energy was set to 35 ± 5 eV.

2.6 Data analysis

The acquired MS raw data files were converted into MGF files by using 5600 ms converter and the MGF files were further searched. MS/MS data were searched against the monkey sequence database from the NCBInr database (release April 2013, containing 29 736 sequences) and the proteins were identified using MASCOT search engine (Matrix Science, London, UK; version 2.3.02). The search was conducted using trypsin as a specific enzyme. A maximum of one missed cleavage was accepted and Gln→pyro-Glu (N-term Q), Oxidation (M), iTRAQ8plex (Y) were chosen as variable modifications. The data acquired from the Triple TOF 5600 mass spectrometer were searched with a fragment mass tolerance of 0.1 Da and a peptide mass tolerance of 0.05 Da. The charge states of peptides were set to +2 and +3. An automatic decoy database search was carried out in MASCOT through choosing the decoy checkbox in which a random sequence of database was generated and tested for raw spectra and the real database. Peptide spectra matches were confirmed through percolator based on *q*-values at a false discovery rate of 0.6% [19]. Peptide identifications were grouped into proteins according to the law of parsimony and filtered to 0.6% false discovery rate [20]. Each of the confident protein identification involves at least two peptides and only unique peptides were used to quantify proteins. The quantitative protein ratios were weighted and normalized by the median ratio in MASCOT. For accurate comparison between samples, fold change > 1.5 or <0.667 and a *p*-value < 0.05 were considered as significantly different expressions according to the *t*-test. Bioinformatics analysis was conducted using Ingenuity Pathway Analysis software (IPA, www.ingenuity.com), GO, and UniProt.

2.7 IFA

Vero cells were seeded on glass coverslips (NEST Biotechnology) that had been placed in 24-well plates until cultures were 70–80% confluent. Cells were infected with PEDV (multiplicity of infection = 0.1) and fixed with cold 4% paraformaldehyde at 12, 18, 24, 30, and 36 hpi, respectively. The PEDV-infected cells were detected using a mouse monoclonal antibody directed against the PEDV N protein and FITC-conjugated goat anti-mouse IgG antibody (Sigma). Cell nuclei were counterstained with 0.01% DAPI (Invitrogen). The fluorescent images were examined by using a confocal laser scanning microscope (LSM 510 Meta, Carl Zeiss).

2.8 Western blot analysis

We chose to analyze hydroxysteroid dehydrogenase like 2 (HSDL2), tyrosine 3-monooxygenase/tryptophan 5-monooxygenase activation protein (14-3-3) gamma, and HSPB1 (HSP27) by Western blotting as significant changes in their protein expression levels were observed. Cell lysates for PEDV- and mock-infected cultures were harvested at 24 hpi and protein concentrations determined. Equivalent quantities of cell lysates were from the three independent biological replicates denatured in 5× sample loading buffer by heating at 100°C for 10 min and separated by 12% SDS-PAGE. Separated proteins were electroblotted onto 0.45 μm PVDF membranes (Millipore, Billerica, MA, USA) and blocked with 10% w/v skim milk in Tris-buffered saline containing Tween 20 for 2 h at room temperature. Membranes were incubated with a rabbit polyclonal antibody against HSDL2, 14-3-3 gamma, and HSP27 (Proteintech, China) at 4°C overnight. After washing three times with Tris-buffered saline containing Tween 20, membranes were incubated with the appropriate HRP-conjugated secondary antibodies (Beyotime, China) at 37°C for 1 h. Detection was performed using Clarity ECL reagents (Bio-Rad, Hercules, CA, USA).

3 Results

3.1 PEDV propagation in Vero cells

The kinetics of PEDV propagation in Vero cells was determined by monitoring CPE and viral protein expression, as well as viral titers at 12, 18, 24, 30, and 36 hpi. As shown in Fig. 1A, minimal CPE was visible at 18 hpi and obvious CPE

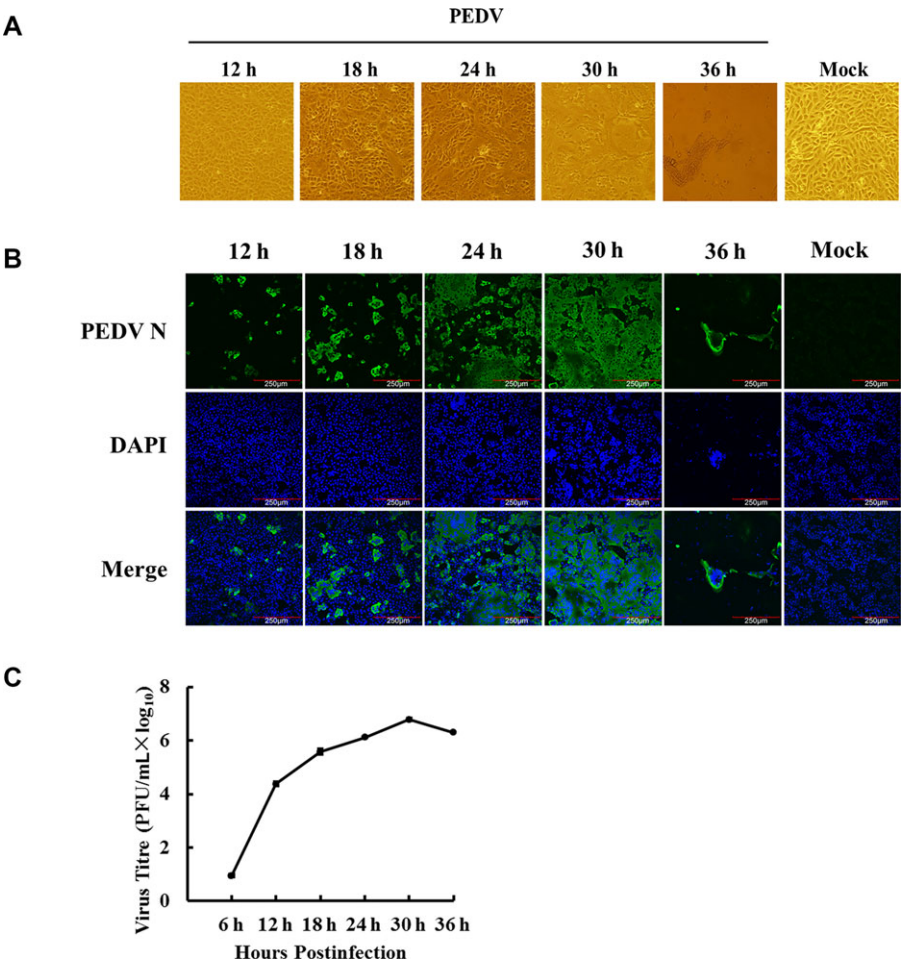

Figure 1. PEDV infection in Vero cells. (A) The cytopathic effects (CPE) of Vero cells at 12, 18, 24, 30, and 36 h after PEDV infection, and mock-infected cells at 36 h as a control. (B) Dynamics of PEDV proliferation by immunofluorescence staining in the infected Vero cells at 12, 18, 24, 30, and 36 h postinfection, respectively, and mock-infected cells at 36 h as a control. (C) One-step growth curve of PEDV strain AJ1102 in Vero cells.

could be observed at 30 hpi; at 36 hpi, almost all cells fell off. The results of IFA for detecting the expression of PEDV N protein showed that the majority of cells were infected at 24 hpi (Fig. 1B). The one-step growth curve showed that viral titer reached to 6.1 $\log_{10}$ at 24 hpi, peaked at 6.8 $\log_{10}$ at 30 hpi, and then gradually declined (Fig. 1C). To make sure higher proportion of the infected cells and to avoid excessive CPE, we thus chose 24 hpi as the time point under our infection conditions for further proteomic analysis.

3.2 Analysis of the differentially regulated proteins

Protein extracts were prepared from PEDV- and mock-infected Vero cells, and then treated as described in Section 2. We detected and quantified 3418 proteins, of which 8 were significantly upregulated and 41 downregulated based on our criteria for the identification of differentially expressed proteins. Among these 49 proteins, 45 proteins have at least two unique peptides, while 4 proteins (mitogen-activated protein kinase 3-like (MAPK3), adenylyl cyclase associated protein 1 isoform 2, alpha-enolase isoform 3, transportin-2-like) have only one unique peptide and one nonunique peptide. The annotated tandem mass spectra and the detailed information regarding protein assignments based on single-peptide assignments of the four proteins are provided as Supporting Information Data 1.

The molecular functional classes and subcellular locations of the 49 differentially expressed proteins were analyzed using UniProt and the GO database (Supporting Information Table 1). The eight upregulated proteins in infected cells were localized to the membrane (one molecule), mitochondria (three molecules), nucleus (two molecules), membrane and mitochondria (one molecule), and cytoplasm and nucleus (one molecule). The 41 downregulated proteins were located in the cytoplasm and nucleus (12 molecules), cytoplasm (6 molecules), ribosome (5 molecules), unknown cellular location (4 molecules), cytoskeleton (4 molecules), nucleus (3 molecules), membrane (2 molecules), cytoplasm and membrane (2 molecules), cytoplasm, extracellular and nucleus (2 molecules), and mitochondrion and nucleus (1 molecule).

Based on gene identifications of the proteins in Table 1, protein GI numbers and ratios (infection/control) were imported into the IPA tool. Their functional classification and interacting pathways were analyzed and reconstructed based on the underlying biological evidence from the literature.

Table 1. Statistically significant differentially expressed proteins identified by iTRAQ analysis of Vero cells infected with PEDV

Protein name	Accession no.	Ratios (infection/ control)	Peptides	Sequence coverage (%)	Functions
Proteins present in increased abundance in PEDV-infected cells					
Glucosidexylosyltransferase 1 isoform 1	gi|109096177	2.042	2	4.5	UDP-xylosyltransferase activity
Hydroxysteroid dehydrogenase like 2 isoform 4	gi|109110554	1.979	4	17.7	Oxidoreductase activity
Metaxin-1 like	gi|297280200	1.654	2	5.1	Protein transport
Single-stranded DNA-binding protein, mitochondrial isoform 1	gi|109068491	1.568	6	44.6	Single-stranded DNA binding
Transportin-2 like	gi|297276226	1.557	2	1.7	Protein transport
Phosphate carrier protein, mitochondrial isoform 1	gi|297263324	1.547	2	5.5	Phosphate ion carrier activity
Pentatricopeptide repeat containing protein 1 like	gi|297287945	1.539	2	3.1	tRNA processing
Small nuclear ribonucleoprotein E like isoform 2	gi|109018742	1.507	2	25	Histone 3′-end processing
Proteins present in decreased abundance in PEDV-infected cells					
Acetyl-CoA acetyltransferase, cytosolic like	gi|297292010	0.666	2	10.9	Acetyl-CoAC-acetyltransferase activity
NSFL1 cofactor p47 like isoform 7	gi|109092580	0.664	6	23.1	Lipid binding
39S ribosomal protein L24, mitochondrial like isoform 1	gi|109017398	0.656	3	17.1	Structural constituent of ribosome
Ran-specific GTPase-activating protein like	gi|297260581	0.654	3	22.5	GDP-dissociation inhibitor activity
14-3-3 Protein eta isoform 2	gi|109093926	0.651	6	30.5	Adapter protein implicated in the regulation of signaling pathways
Protein-L-isoaspartate (D-aspartate) O-methyltransferase like	gi|297284352	0.651	3	21.1	Protein-L-isoaspartate (D-aspartate) O-methyltransferase activity
Dipeptidyl peptidase 3 like, partial	gi|109109554	0.649	2	36.9	Dipeptidyl-peptidase activity
Small acidic protein like	gi|109107167	0.648	3	21.9	Unknown
Gamma interferon inducible protein 16 like isoform 2	gi|109017483	0.648	3	6.3	Double-stranded DNA binding
Caspase-8	gi|297264681	0.643	2	10	Induced cell death
High-mobility group protein B1 like	gi|109098276	0.642	3	17.7	DNA binding, bending
14-3-3 Protein theta isoform 1	gi|109075480	0.639	7	37.1	Adapter protein implicated in the regulation of signaling pathways
HSP beta-1	gi|109066218	0.637	4	31.2	Response to stress
Gamma-enolase isoform 1	gi|109095369	0.634	7	23.7	Magnesium ion binding
UV excision repair protein RAD23 homolog B isoform 5	gi|109110657	0.632	5	21.8	Nucleotide-excision repair
SH3 domain binding glutamic acid rich like protein like	gi|297304256	0.632	2	19.3	Protein disulfide oxidoreductase activity
Gelsolin isoform 13	gi|109110383	0.631	8	15.9	Calcium ion binding
60S ribosomal protein L24 isoform 2	gi|109032850	0.631	3	19.1	Structural constituent of ribosome
Multiple coagulation factor deficiency protein 2 like isoform 1	gi|297265949	0.63	2	28.1	Vesicle-mediated transport
Protein TFG isoform 2	gi|109032777	0.628	4	19.8	Signal transducer activity
Phosphoglyceratemutase 1 isoform 2	gi|109100081	0.624	6	37	Phosphoglyceratemutase activity
Myotrophin isoform 3	gi|109068363	0.623	2	20.3	Structural constituent of cytoskeleton
Annexin A3 isoform 3	gi|109074379	0.622	5	19.5	Phospholipase A2 inhibitor activity
Protein phosphatase 1 regulatory subunit 7 like isoform 1	gi|109101715	0.62	4	14.1	Protein phosphatase type 1 regulator activity
Hepatoma-derived growth factor like nucleotide binding	gi|297281928	0.609	2	28.4	Transcription regulation
Far upstream element binding protein 2	gi|297275911	0.597	9	16.6	mRNA trafficking
40S ribosomal protein S24 like isoform 1	gi|109037800	0.59	2	17.7	Structural constituent of ribosome

(Continued)

Table 1. (Continued)

Protein name	Accession no.	Ratios (infection/ control)	Peptides	Sequence coverage (%)	Functions
NudC domain containing protein 3	gi|109066663	0.586	3	12.9	Unknown
Gephyrin isoform 2	gi|109083983	0.577	3	7.2	Structural constituent of cytoskeleton
60S ribosomal protein L27a like	gi|109065734	0.572	3	20.9	Structural constituent of ribosome
14-3-3 Protein beta/alpha	gi|297259739	0.551	5	23.6	Adapter protein implicated in the regulation of signaling pathways
60S ribosomal protein L36 like	gi|109081357	0.549	2	20	Structural constituent of ribosome
Synapse-associated protein 1 like	gi|297305163	0.538	2	14.5	Unknown
14-3-3 Protein gamma like isoform 1	gi|109066214	0.537	5	24.3	Protein kinase C inhibitor activity
Tubulin gamma-1 chain	gi|109115505	0.537	3	10.4	Structural constituent of cytoskeleton
Destrin isoform 1	gi|109092999	0.533	4	33.8	Structural constituent of cytoskeleton
Prostaglandin E synthase 3 like isoform 4	gi|109097318	0.492	4	35.6	Chaperone cofactor dependent protein refolding
Adenylyl cyclase associated protein 1 isoform 2	gi|297278362	0.479	7	26.8	Establishment or maintenance of cell polarity
Coiled-coil domain containing protein 124 like	gi|109123948	0.449	2	14.4	Unknown
Mitogen-activated protein kinase 3 like (MAPK3)	gi|297283792	0.366	2	5.6	Signal transduction
Alpha-enolase isoform 3	gi|109066574	0.277	13	30.6	Transcription corepressor activity

The analysis of function classification by IPA showed that the 8 significantly upregulated and 41 downregulated proteins could be divided among four distinct functional sets: diseases and disorders; molecular and cellular functions; physiological system development; and functions including toxicity functions (Fig. 2 and Supporting Information Table 2). These differentially regulated proteins are involved in biological processes relevant to gene expression, cell cycle, cell signaling, cell death and survival, cellular function, and maintenance.

With goal of exploring the potential protein network connections for the differentially regulated proteins in detail, IPA tool was used. The differentially regulated proteins were mapped to three specific functional networks. Each network had at least five "focus" proteins (significantly up- or downregulated proteins). The three networks of interest correspond to cancer, cell death and survival, cell-to-cell signaling, and interaction (Fig. 3A); cancer, cardiovascular disease, and hereditary disorder (Fig. 3B); RNA post-transcriptional modification, cellular developmental, cellular growth, and proliferation (Fig. 3C).

3.3 Validation of protein identification and quantitation

We analyzed expression levels of HSDL2 (upregulated), 14-3-3 gamma (downregulated), and HSP27 (downregulated) in PEDV-infected Vero cells (Fig. 4) by Western blotting. The proteins were selected on the basis of interest and on their different ratios. The ratios of these three proteins between infected and uninfected cells were consistent with those determined using the iTRAQ labeled LC-MS/MS system.

4 Discussion

Proteomics has become an important methodology for determining cellular protein interactions and host cellular pathophysiological processes following virus infection [12, 21]. To date, no analysis has been reported for the differential proteomes of host cells infected with PEDV. Based on our findings, the expressions of 49 different proteins were significantly altered in PEDV-infected cells. These proteins were involved in a variety of processes including apoptosis, signal transduction, and stress responses of host cells. Our data are overview of the altered proteins during a host response to PEDV infection and should provide clues regarding PEDV pathogenesis.

The apoptosis of host cells plays a major role in regulating the pathogenesis of many infectious diseases [22]. Apoptosis triggered by virus infection directly leads to viral pathogenesis; however, blocking apoptosis can avoid premature death of the infected cells, permitting a high titer of virus replication or a persistent infection [17]. In our analysis, two apoptosis-related genes, (14-3-3 and caspase-8) were identified following PEDV infection. The 14-3-3 proteins constitute a family of conserved adaptor and scaffold proteins present in all eukaryotic organisms. Previous reports showed that 14-3-3 proteins modulate the cell cycle and apoptosis at multiple steps, leading to an inhibition of the onset of apoptosis [23, 24]. Our results demonstrate that decreased expression of four 14-3-3 proteins (eta, theta, beta/alpha, gamma) was concomitant with PEDV infection, and thus predicted to promote apoptosis of infected cells. Caspase-8 is the initiator caspase that is activated by the correlation between external apoptotic elements and cell surface molecules, playing

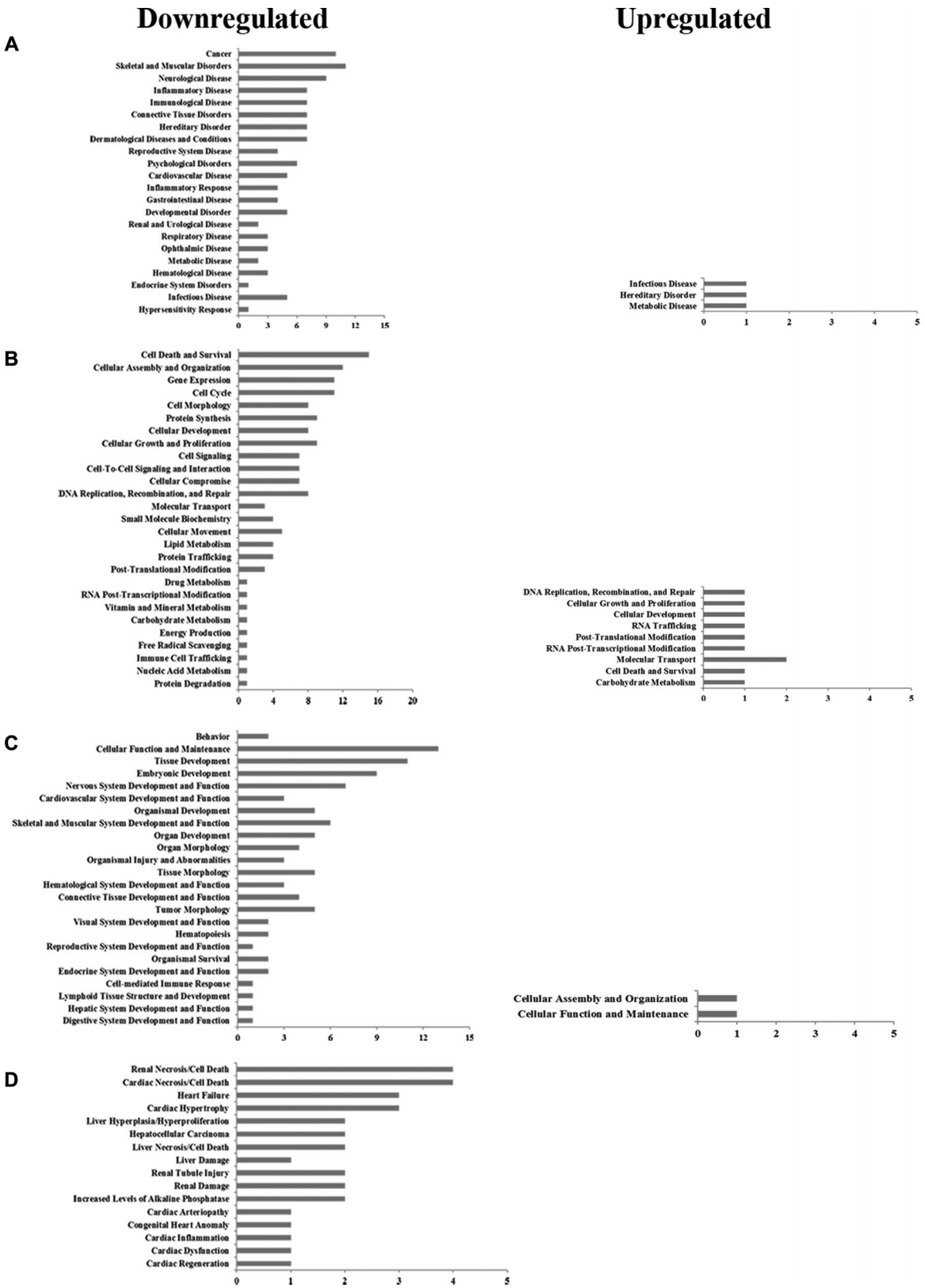

Figure 2. Functional characterization of up- and downregulated proteins. (A) Diseases and disorders. (B) Molecular and cellular functions. (C) Physiological system development and functions. (D) Toxicity functions. More information is available in Supporting Information Table 2.

A Network 1: Cancer, Cell Death and Survival, Cell-To-Cell Signaling and Interaction

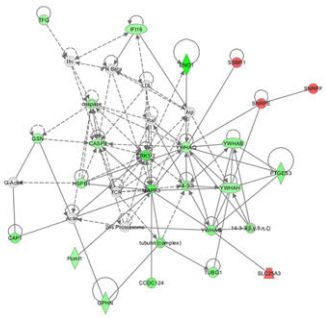

B Network 2: Cancer, Cardiovascular Disease, Hereditary Disorder

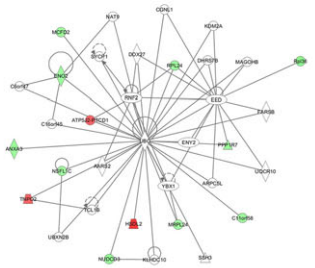

C Network 3: RNA Post-Transcriptional Modification, Cellular Developmental, Cellular Growth and Proliferation

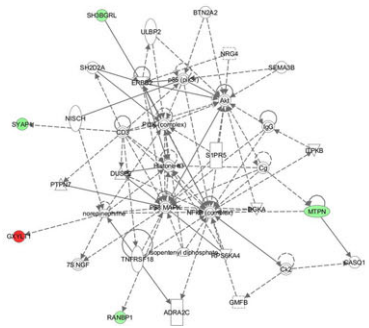

Figure 3. Specific network analysis of proteins significantly altered in PEDV-infected cells. Significantly upregulated proteins are shown in red, significantly downregulated proteins in green, and proteins that were not identified in this study but are involved in the networks are shown in white. The color shade indicates the magnitude of the change in protein expression. Shapes are indicative of the molecular class, and lines with arrows indicate molecular relationships (Supporting Information Fig. 1).

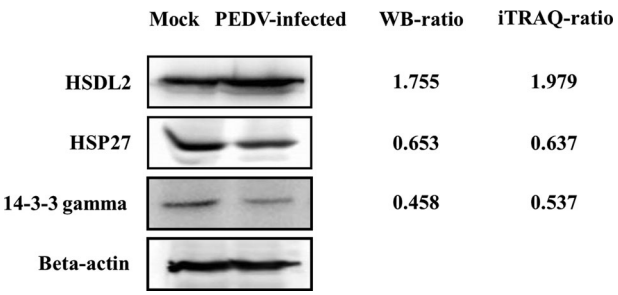

Figure 4. Confirmation of differentially expressed proteins by Western blotting. Analysis of HSDL2, 14-3-3 gamma, and HSP27 expression levels in PEDV-infected and control cells by Western blotting. The WB-ratio (Western blotting ratio, PEDV-infected/mock) was calculated based on the relative intensity of each band in PEDV-infected cells to the corresponding band in mock-infected cells. Beta-actin was used as a loading control. The iTRAQ-ratio (infection/control) obtained by MS analysis are shown on the right.

fundamental roles in initiating the apoptotic cascade response [25]. The downregulation of caspase-8 expression in PEDV-infected cells suggests a mechanism that attenuates virus-induced apoptosis at the early infection phase, thus favoring a virus to replicate to a higher titer. In the case of SARS-CoV, stimulation of both apoptotic and antiapoptotic elements has been seen, allowing for rapid multiplication of progeny virus before cell lysis [26]. The interplay between apoptosis-related genes in PEDV infection might contribute to it achieving maximum viral replication before cell death.

Viruses are known to develop the ability to manipulate a variety of host cellular signal transduction pathways to facilitate virus survival. Among these pathways is the extracellular signal regulated kinases (ERKs) pathway, comprising Raf, MEK1/2, and ERK1/2. These play central roles in the modulation of cell survival, differentiation, and proliferation [27]. Many viruses activate the ERK pathway for higher levels of cellular and viral gene production. By activating ERK1/2, enterovirus 71 prevents activation of the proapoptotic molecules caspase-9 and Bcl-2 associated death promoter [28]. Porcine reproductive and respiratory syndrome virus infection activates ERK1/2 at the early infection phase in PAM cells, with ERK activation essential for porcine reproductive and respiratory syndrome virus replication in vitro [29]. Some studies have shown a negative correlation between ERK activity and viral replication. The Ebola virus glycoprotein GP specifically inhibits ERK1/2 to cause increased cell toxicity and viral titers [30]. Yoshizuka et al. reported that overexpression of the human immunodeficiency virus (HIV) type 1 (HIV-1) Vpr protein downregulated gene expression and phosphorylation of ERK1/2 in the ERK/MAPK pathway. It was speculated that the decrease in ERK1/2 activation is important for HIV replication and pathogenesis [31]. SARS-CoV N induces apoptosis of COS-1 monkey kidney cells in the absence of growth factors through downregulation of the ERK pathway [32]. ERK1/2 regulation of viral replication functions occurs at specific points during the replication cycle [33]. The manipulation of the ERK pathway is a ubiquitous characteristic during viral infection and is not limited to specific viruses or viral events [34]. In our study, ERK1 was significantly downregulated during PEDV infection. The specific

mechanism by which PEDV manipulates the ERK pathway for maximal viral replication is currently under investigation in our laboratory.

Activation of the heat-shock response might be a specific function that a virus exerts to guarantee appropriate synthesis of viral proteins [35]. In our study, HSP27 was significantly downregulated in Vero cells following PEDV challenge. HSP27, a ubiquitous stress-inducible cellular protein, is a multifunctional protein that plays a role in the inhibition of caspase-independent apoptosis, actin cytoskeletal remodeling, and might also participate in protein degradation [36,37]. It has been implicated that HSP27 is upregulated during enterovirus 71, feline herpesvirus, and infectious bursal disease virus infections [38–40]. Based on our results, HSP27 was downregulated during PEDV infection, similar to previous reports regarding adenoviruses [41], classical swine fever virus [42], and porcine circovirus type 2 [21]. HSP27 is an intracellular antiviral factor against hepatitis B virus through the induction of type I interferon and downstream antiviral effectors [43] and inhibits caspase-independent apoptosis. We suspected that decreased expression of HSP27 might have a specific role in host cells during viral infection, however that specific mechanism requires further investigation.

In summary, the proteomic changes in PEDV-infected Vero cells were characterized using iTRAQ combined with LC-MS/MS. To the best of our knowledge, this is the first time proteomics has been used to explore the pathogen–host protein interaction network in PEDV-infected Vero cells. Since the PEDV variant emerged in China and the United States, PEDV has received increasing attention, and more researchers have undertaken the study of PEDV. Our analyses of the proteins discussed above were descriptive, and further functional investigations are required to elucidate the pathogenic mechanisms and cellular responses to PEDV infection. Such molecular insights into differentially expressed cellular proteins would be helpful in studying the infectivity and pathogenesis of PEDV.

This work was supported by the Key Technology R&D Programme of China (2015BAD12B02), the Natural Science Foundation of Hubei Province (2014CFA009), the National Natural Sciences Foundation of China (31402239), and the Fundamental Research Funds for the Central Universities (2013PY043).

The authors have declared no conflict of interest.

5 References

[1] Junwei, G., Baoxian, L., Lijie, T., Yijing, L., Cloning and sequence analysis of the N gene of porcine epidemic diarrhea virus LJB/03. *Virus Genes* 2006, *33*, 215–219.

[2] Wood, E. N., An apparently new syndrome of porcine epidemic diarrhoea. *Vet. Rec.* 1977, *100*, 243–244.

[3] Chasey, D., Cartwright, S. F., Virus-like particles associated with porcine epidemic diarrhoea. *Res. Vet. Sci.* 1978, *25*, 255–256.

[4] Li, W., Li, H., Liu, Y., Pan, Y. et al., New variants of porcine epidemic diarrhea virus, China, 2011. *Emerg. Infect. Dis.* 2012, *18*, 1350–1353.

[5] Bi, J., Zeng, S., Xiao, S., Chen, H., Fang, L., Complete genome sequence of porcine epidemic diarrhea virus strain AJ1102 isolated from a suckling piglet with acute diarrhea in China. *J. Virol.* 2012, *86*, 10910–10911.

[6] Wang, X. M., Niu, B. B., Yan, H., Gao, D. S. et al., Genetic properties of endemic Chinese porcine epidemic diarrhea virus strains isolated since 2010. *Arch. Virol.* 2013, *158*, 2487–2494.

[7] Chen, J., Liu, X., Shi, D., Shi, H. et al., Complete genome sequence of a porcine epidemic diarrhea virus variant. *J. Virol.* 2012, *86*, 3408.

[8] Sun, R. Q., Cai, R. J., Chen, Y. Q., Liang, P. S. et al., Outbreak of porcine epidemic diarrhea in suckling piglets, China. *Emerg. Infect. Dis.* 2012, *18*, 161–163.

[9] Chen, Q., Li, G., Stasko, J., Thomas, J. T. et al., Isolation and characterization of porcine epidemic diarrhea viruses associated with the 2013 disease outbreak among swine in the United States. *J. Clin. Microbiol.* 2014, *52*, 234–243.

[10] Stevenson, G. W., Hoang, H., Schwartz, K. J., Burrough, E. R. et al., Emergence of Porcine epidemic diarrhea virus in the United States: clinical signs, lesions, and viral genomic sequences. *J. Vet. Diagn. Invest.* 2013, *25*, 649–654.

[11] Cho, W. K., Kim, H., Choi, Y. J., Yim, N. H. et al., Epimedium koreanum Nakai water extract exhibits antiviral activity against porcine epidermic diarrhea virus in vitro and in vivo. *Evid. Based Complement. Alternat. Med.* 2012, *2012*, 985151. doi: 10.1155/2012/985151.

[12] Maxwell, K. L., Frappier, L., Viral proteomics. *Microbiol Mol Biol Rev.* 2007, *71*, 398–411.

[13] Munday, D. C., Surtees, R., Emmott, E., Dove, B. K. et al., Using SILAC and quantitative proteomics to investigate the interactions between viral and host proteomes. *Proteomics* 2012, *12*, 666–672.

[14] Zeng, R., Ruan, H. Q., Jiang, X. S., Zhou, H. et al., Proteomic analysis of SARS associated coronavirus using two-dimensional liquid chromatography mass spectrometry and one-dimensional sodium dodecyl sulfate-polyacrylamide gel electrophoresis followed by mass spectroemtric analysis. *J. Proteome Res.* 2004, *3*, 549–555.

[15] Sun, J., Han, Z., Shao, Y., Cao, Z. et al., Comparative proteome analysis of tracheal tissues in response to infectious bronchitis coronavirus, Newcastle disease virus, and avian influenza virus H9 subtype virus infection. *Proteomics* 2014, *14*, 1403–1423.

[16] Zhang, X., Shi, H. Y., Chen, J. F., Shi, D. et al., Identification of cellular proteome using two-dimensional difference gel electrophoresis in ST cells infected with transmissible gastroenteritis coronavirus. *Proteome Sci.* 2013, *11*, 31.

[17] Enjuanes, L., Almazan, F., Sola, I., Zuniga, S., Biochemical aspects of coronavirus replication and virus-host interaction. *Annu. Rev. Microbiol.* 2006, *60*, 211–230.

[18] Hofmann, M., Wyler, R., Propagation of the virus of porcine epidemic diarrhea in cell culture. *J. Clin. Microbiol.* 1988, *26*, 2235–2239.

[19] Wright, J. C., Collins, M. O., Yu, L., Kall, L. et al., Enhanced peptide identification by electron transfer dissociation using an improved Mascot Percolator. *Mol. Cell. Proteomics* 2012, *11*, 478–491.

[20] Nesvizhskii, A. I., Aebersold, R., Interpretation of shotgun proteomic data: the protein inference problem. *Mol. Cell. Proteomics* 2005, *4*, 1419–1440.

[21] Zhang, X., Zhou, J., Wu, Y., Zheng, X. et al., Differential proteome analysis of host cells infected with porcine circovirus type 2. *J. Proteome Res.* 2009, *8*, 5111–5119.

[22] Johns, H. L., Bensaude, E., LaRocca, S. A., Seago, J. et al., Classical swine fever virus infection protects aortic endothelial cells from pIpC-mediated apoptosis. *J. Gen. Virol.* 2010, *91*, 1038–1046.

[23] vanHemert, M. J., Steensma, H. Y., vanHeusden, G. P., 14-3-3 proteins: key regulators of cell division, signalling and apoptosis. *Bioessays* 2001, *23*, 936–946.

[24] Xing, H., Zhang, S., Weinheimer, C., Kovacs, A., Muslin, A. J., 14-3-3 proteins block apoptosis and differentially regulate MAPK cascades. *EMBO J.* 2000, *19*, 349–358.

[25] Cohen, G. M., Caspases: the executioners of apoptosis. *Biochem. J.* 1997, *326*(Pt 1), 1–16.

[26] Tang, B. S., Chan, K. H., Cheng, V. C., Yuen, K. Y., Comparative host gene transcription by microarray analysis early after infection of the Huh7 cell line by SARS coronavirus and human coronavirus 229E. *Hong Kong Med. J.* 2009, *15*(Suppl 9), 23–26.

[27] Fang, J. Y., Richardson, B. C., The MAPK signalling pathways and colorectal cancer. *Lancet Oncol.* 2005, *6*, 322–327.

[28] Wong, W. R., Chen, Y. Y., Yang, S. M., Chen, Y. L., Horng, J. T., Phosphorylation of PI3K/Akt and MAPK/ERK in an early entry step of enterovirus 71. *Life Sci.* 2005, *78*, 82–90.

[29] Lee, Y. J., Lee, C., Porcine reproductive and respiratory syndrome virus replication is suppressed by inhibition of the extracellular signal-regulated kinase (ERK) signaling pathway. *Virus Res.* 2010, *152*, 50–58.

[30] Zampieri, C. A., Fortin, J. F., Nolan, G. P., Nabel, G. J., The ERK mitogen-activated protein kinase pathway contributes to Ebola virus glycoprotein-induced cytotoxicity. *J. Virol.* 2007, *81*, 1230–1240.

[31] Yoshizuka, N., Yoshizuka-Chadani, Y., Krishnan, V., Zeichner, S. L., Human immunodeficiency virus type 1 Vpr-dependent cell cycle arrest through a mitogen-activated protein kinase signal transduction pathway. *J. Virol.* 2005, *79*, 11366–11381.

[32] Surjit, M., Liu, B., Jameel, S., Chow, V. T., Lal, S. K., The SARS coronavirus nucleocapsid protein induces actin reorganization and apoptosis in COS-1 cells in the absence of growth factors. *Biochem. J.* 2004, *383*, 13–18.

[33] Cai, Y., Liu, Y., Zhang, X., Suppression of coronavirus replication by inhibition of the MEK signaling pathway. *J. Virol.* 2007, *81*, 446–456.

[34] Moser, L. A., Schultz-Cherry, S., Suppression of astrovirus replication by an ERK1/2 inhibitor. *J. Virol.* 2008, *82*, 7475–7482.

[35] Glotzer, J. B., Saltik, M., Chiocca, S., Michou, A. I. et al., Activation of heat-shock response by an adenovirus is essential for virus replication. *Nature* 2000, *407*, 207–211.

[36] Vidyasagar, A., Wilson, N. A., Djamali, A., Heat shock protein 27 (HSP27): biomarker of disease and therapeutic target. *Fibrogenesis Tissue Repair* 2012, *5*, 7.

[37] Ciocca, D. R., Oesterreich, S., Chamness, G. C., McGuire, W. L., Fuqua, S. A., Biological and clinical implications of heat shock protein 27000 (Hsp27): a review. *J. Natl. Cancer Inst.* 1993, *85*, 1558–1570.

[38] Leong, W. F., Chow, V. T., Transcriptomic and proteomic analyses of rhabdomyosarcoma cells reveal differential cellular gene expression in response to enterovirus 71 infection. *Cell Microbiol.* 2006, *8*, 565–580.

[39] Zheng, X., Hong, L., Shi, L., Guo, J. et al., Proteomics analysis of host cells infected with infectious bursal disease virus. *Mol. Cell. Proteomics* 2008, *7*, 612–625.

[40] Go, E. P., Wikoff, W. R., Shen, Z., O'Maille, G. et al., Mass spectrometry reveals specific and global molecular transformations during viral infection. *J. Proteome Res.* 2006, *5*, 2405–2416.

[41] Zantema, A., deJong, E., Lardenoije, R., vander Eb, A. J., The expression of heat shock protein hsp27 and a complexed 22-kilodalton protein is inversely correlated with oncogenicity of adenovirus-transformed cells. *J. Virol.* 1989, *63*, 3368–3375.

[42] Sun, J., Jiang, Y., Shi, Z., Yan, Y. et al., Proteomic alteration of PK-15 cells after infection by classical swine fever virus. *J. Proteome Res.* 2008, *7*, 5263–5269.

[43] Tong, S. W., Yang, Y. X., Hu, H. D., An, X. et al., HSPB1 is an intracellular antiviral factor against hepatitis B virus. *J. Cell Biochem.* 2013, *114*, 162–173.

